01 Jan 2021

Microsphere Photolithography Patterned Nanohole Array on an Optical Fiber

Ibrahem Jasim

Jiayu Liu

Chen Zhu

Muhammad Roman

et. al. For a complete list of authors, see https://scholarsmine.mst.edu/ele_comeng_facwork/4405

Recommended Citation

I. Jasim et al., "Microsphere Photolithography Patterned Nanohole Array on an Optical Fiber," *IEEE Access*, vol. 9, pp. 32627-32633, article no. 3059439, Institute of Electrical and Electronics Engineers (IEEE), Jan 2021.

The definitive version is available at https://doi.org/10.1109/ACCESS.2021.3059439

IEEE Access
Multidisciplinary | Rapid Review | Open Access Journal

Received December 21, 2020, accepted January 21, 2021, date of publication February 15, 2021, date of current version March 2, 2021.

Digital Object Identifier 10.1109/ACCESS.2021.3059439

Microsphere Photolithography Patterned Nanohole Array on an Optical Fiber

IBRAHEM JASIM[1], JIAYU LIU[1], CHEN ZHU[2], MUHAMMAD ROMAN[3], JIE HUANG[3], (Senior Member, IEEE), EDWARD KINZEL[2], AND MAHMOUD ALMASRI[1]

[1]Department of Electrical Engineering and Computer Science, University of Missouri, Columbia, MO 65211, USA
[2]Department of Aerospace and Mechanical Engineering, University of Notre Dame, Notre Dame, IN 46556, USA
[3]Department of Electrical and Computer Engineering, Missouri University of Science and Technology, Rolla, MO 65409, USA

Corresponding author: Mahmoud Almasri (almasrim@missouri.edu)

This work was supported in part by the Applied Optoelectronics Inc. (AOI), and in part by the NSF Civil, Mechanical and Manufacturing Innovation (CMMI) under Grant 1653792.

ABSTRACT Microsphere Photolithography (MPL) is a nanopatterning technique that utilizes a self-assembled monolayer of microspheres as an optical element to focus incident radiation inside a layer of photoresist. The microspheres produces a sub-diffraction limited photonic-jet on the opposite side of each microsphere from the illumination. When combined with pattern transfer techniques such as etching/lift-off, MPL provides a versatile, low-cost fabrication method for producing hexagonal close-packed metasurfaces. This article investigates the MPL process for creating refractive index (RI) sensors on the cleaved tips of optical fiber. The resonant wavelength of metal elements on the surface is dependent on the local dielectric environment and allows the refractive index of an analyte to be resolved spectrally. A numerical study of hole arrays defined in metal films shows that the waveguide mode provides good sensitivity to the analyte refractive index. This can be readily tuned by adjusting the MPL exposure and the simulation results guide the fabrication of a defect tolerant refractive index sensor on the tip of a fiber tip with a sensitivity of 613 nm/RIU. The conformal nature of the microsphere monolayer simplifies the fabrication process and provides a viable alternative to direct-write techniques such as Focused Ion Beam (FIB) milling.

INDEX TERMS Fiber tip, refractive index, microsphere photolithography.

I. INTRODUCTION

Optical refractive index (RI) sensing is widely used in chemistry and biology for label-free detection. Metal-based plasmonic [1]–[4] and dielectric-based optical [5]–[8] designs produce a resonant frequency that depends on the refractive index of an analyte. The performance of these sensors is characterized by their sensitivity, $S = \Delta\lambda_0/\Delta n$, which describes the shift of the resonant wavelength with respect to the change in the refractive index of the analyte. The ability to resolve the resonant wavelength is also affected by its full width at half maximum (FWHM), and a figure of merit for RI sensors is $FOM = S/FWHM$ [9]. Propagating Surface Plasmon Resonance (PSPR) sensors have sensitivities as high as 2×10^6 nm/RIU [10] due to the large penetration depth of the evanescent field into the dielectric medium [11], [12]. However, this comes at the expense of a relatively large interrogation areas. Local Surface Plasmon Resonance (LSPR) sensors have lower sensitivity but a confined interrogation volume which provides a greater spatial resolution of the analyte. The theoretical limit for the sensitivity of LSPR sensors is proportional to the ratio between the resonant wavelength and index of refraction, λ_0/n [12]. Sensitivities of 1000 nm/RIU are typical [13]–[16] and can be further improved by introducing Fano resonances with dark modes [17]. This article focuses on the physics and demonstration of the sensitivity without using any recognition layer. Biorecognition layer will be added in the future to improve the sensitivity. In addition, most of the techniques found in literature require different fabrication process such Focused Ion Beam (FIB) and Electron Beam Lithography (EBL) which is much more complicated and expensive. On the contrary, the MPL is a much-simplified and cost-effective method.

Optical fiber provides an ideal platform for LSPR RI sensors because the advantage of local interrogation is integrated with illumination/collection. This facilitates greater flexibility, remote sensing, and light weight compared to free-space coupling options. These attributes are particularly useful for

The associate editor coordinating the review of this manuscript and approving it for publication was Sukhdev Roy.

microfluidics and in-vivo access. RI sensors have been patterned either on the sidewall of optical fiber [18], fiber tip or facet [19]–[27] or both [28], [29] for transmission/reflection measurements. For sensors on the tip of the optical fiber, reflection-based measurements only require one port into the sensing media, and the interrogation area has been shown to approach the area of the fiber core (as small as 1/2500 mm^2 for single mode fiber) [21].

Focused Ion Beam (FIB) and Electron Beam Lithography (EBL) are the most common methods to pattern RI sensors on the facet of optical fiber [30]. For example, Lan *et al.* [21] demonstrated FIB milling a square lattice of subwavelength holes on the tip of optical fiber to achieve a sensitivity of 573 nm/RIU and Lin *et al.* [23] patterned nanodots using EBL to produce sensors with 196 nm/RIU. The cost of patterning is a significant obstacle to the practical use of optical fiber-based LSPR sensors. While versatile, the direct-write techniques do not scale well for mass production of sensors. The required feature sizes and alignment to multiple fibers challenge conventional lithography. This has motivated the investigation of several alternative patterning techniques for defining nanoscale geometry on an optical fiber such as nano-imprint lithography [31] and Nanosphere Lithography (NSL) [32]. The nanoimprint lithography involves creating a nanostructure template that can be transferred into the substrate using a transparent curing adhesion layer along with applied pressure. The nanoimprint techniques have some drawbacks such as nanoscale mask misalignment due to the small area of the fiber core [19] in addition to the complexity and high cost of implementation. NSL uses a self-assembled layer of nano or micro spheres on the substrate to create periodic nano structures. The assembled nanospheres is followed by etching and/or material deposition. This approach has been used to create nanostars or nanoholes structures [32]. NSL can create some different structures by extra pre-treatment. However, the number of these structures are limited due to the nature of NSL technique. Meanwhile, Microsphere Photolithography (MPL) is very versatile in creating complicated resonators (e.g. SRRs or dipole structures). Basically, microspheres in MPL method work as a ball lens array that images incident collimated UV radiation to a sub-diffraction limited photonic jet. In addition, there is a possibility that the microspheres can be recycled as opposed to being consumed as a shadow/etch mask.

This article reports on the use of Microsphere Photolithography (MPL) for the patterning RI sensor on the fiber tip. Microsphere photolithography is capable of fabricating structures featured with highly ordered periodic structures in 2D [33]–[36]. The self-assembled microsphere array is used as an optical element and focuses UV flood illumination to sub-diffraction limited photonic nanojets within the photoresist. This near-field permits the facile patterning of sub-200 nm features. Combined with positive/negative tone photoresist and etching/lift-off technique, this method was capable of fabricating nanopillar/hole array that meets the requirement of the refractive index sensor. Compared to NSL, the MPL utilizes microsphere as an optical element instead of using Physical Vapor Deposition (PVD) or etching masks, offers a wide versatility for fabrication by creating different nanoholes and nanodisks structure through controlling the incident UV illumination [37]. Both MPL and NSL methods may suffer from making a SAM (Self-Assembly Monolayer) a single crystal for a large surface area on a glass substrate. One drawback of the MPL is the need to deposit a uniform thin layer of photoresist over small sized substrates such as the fiber tip. With MPL (as well as NSL) the self-assembly of the microspheres can result in the grain boundaries in HCP lattice. Disruptions in the lattice have the potential to disrupt the long-range order of the pattern and frustrate PSPR modes. This is less of an issue for the fiber tip platform because of the small surface area. Studies on MPL process have been presented in various papers [33], [34], [38]–[42], The contribution of this article is, implementing MPL on fiber tips.

This article presents a procedure for fabricating a nanohole array on aluminum film of the optical fiber tip using microsphere photolithography. The MPL technique allows the size of the holes to be controlled by adjusting the exposure dose and this relationship is characterized experimentally. This allows the resonant wavelength of the sensor to be engineered. Electromagnetic modeling is used to understand the effects of the geometrical parameters on the sensor performance. These results predict that the sensitivity is maximized for a coupled waveguide mode in the holes. Experimental results are in good agreement with the simulation and provide a measured sensitivity of 613 nm/RIU for glucose dissolved in water. Overall, the results show that MPL has the potential for a practical, low-cost fabrication approach for RI sensors.

II. MICROSPHERE PHOTOLITHOGRAPHY PATTERNING PROCESS

Single-mode fiber (Corning SMF-28) with an 8.2 μm diameter core and 125 μm cladding are used throughout this work. A layer of aluminum was deposited with a thickness of 50 nm, using an E-beam evaporator, on the fiber/ferrule after polishing (successively polishing using 5 μm, 3 μm, 1 μm, 0.3 μm carbide polishing paper to reduce the surface roughness)/cleaning (before spin-coating). After polishing, each fiber was carefully inspected with microscope to make sure the surface is clean and smooth. Coating a uniform layer of photoresist on the small surface area of the fiber end-facet can be challenging in a laboratory prototyping environment using spin coating. Surface tension leads to an edge bead with a non-uniform photoresist thickness. This is overcome by shifting the edge further away from the core by securing the fiber in a ceramic ferrule with a 125 μm inner diameter. The jacket is first removed from the first 1.5 cm of a 10 cm long of the fiber. The stripped end is positioned in the ferrule, so the cleaved face is even with the face of the ferrule. A small amount of glue is used to secure the fiber and cured by baking for 10 minutes at 100 °C on a hot plate. The tip of the ferrule/fiber is then polished and cleaned to provide a clean

and smooth fiber end surface. The ferrule is then placed in a small 3D printed chuck, which allows the assembly to be secured on a spin coater. Shipley 1805 photoresist is then spun onto the polished tip/ferrule to provide a photoresist layer with a thickness of 400 nm (The surface tension due to small area of the fiber tip caused this number to be different from the data provided by manufacturer). After spin coating, the ferrule is removed from the chuck and placed on a fixture which is submerged in a water-filled beaker.

Dry silica microspheres (Sigma Aldrich) with a diameter of $p = 1\mu$m and a coefficient of variance of less than 3% are dispersed in butanol to a concentration of 1 mg/mL with 5 mg of surfactant (Sodium lauryl sulfate). Ultrasonication is used to ensure that the microsphere/butanol suspension is monodisperse. One drop (2 μL) of the microsphere suspension is dispensed onto the surface of the water-filled beaker by a syringe. The ratio of the microsphere suspension to the water surface area is 0.25 μL/cm^2 which is less than maximum concentration if the entire surface was covered with a monolayer of microspheres (0.25 μL/cm^2). Capillary forces cause the microspheres to rapidly self-assemble on a close-packed lattice on the surface of the water. Sphere self-assemble is a natural process. We cannot control the sphere orientation and number of defects during self-assembly process. However, the defect we observed on the fiber tip were minimum. This is due to the small surface area of the fiber tip. We have tested many fibers with identical feature. All these fibers showed similar performance with a minimum change of the signal peak. In addition, the simulation shows that the orientation doesn't have an effect on the performance as well. Following the self-assembly of the microsphere array, water is withdrawn slowly from the beaker by a faucet located at the bottom of the beaker. Eventually, the surface of the water impinges on the submerged fiber surface, and the microsphere lattice is transferred on the photoresist covered fiber surface [42].

After transferring the microsphere array, the fiber/ferrule is removed from the water and the assembly is dried at room temperature. The sample is then exposed by flood illuminating with the microspheres at normal incidence using an MA6 mask-aligner. This provides spatially uniform, collimated UV radiation at $\lambda = 365$ nm (i-line) with an irradiance is 7 mW/cm^2. Each microsphere generates a photonic jet in the photoresist. After exposure, the fiber/ferrule is placed in developer (MF 319) for 60 s (400 nm photoresist thickness). The microspheres are removed in the developer.

The developed photoresist can be used as a mask for metal etching (deposited on the fiber/ferrule prior to spin-coating the photoresist), or as a sacrificial layer for lift-off process. Figure 1 illustrates the MPL fabrication approach used for the sensors in this article. After the MPL process, the fiber/ferrule is immersed in the aluminum etchant for 30 s. The etchant removes the exposed aluminum to open holes in the aluminum layer. After etching, the photoresist is removed using acetone. The reason we used aluminum is because it is less expensive, and we selected it on the basis of creating low-cost

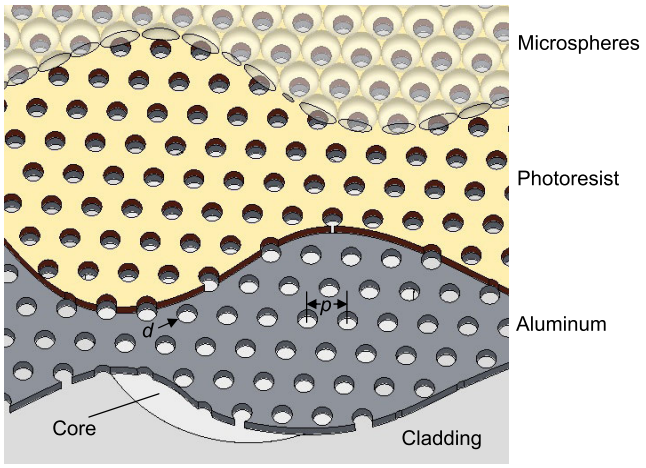

FIGURE 1. Schematic of hole pattern on fiber tip: the upper part shows the microsphere assembled on the fiber tip before exposure, (photoresist layer was ignored in the schematic); the lower part shows the al hole pattern after etching.

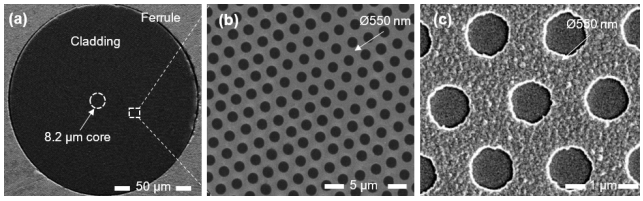

FIGURE 2. SEM Micrographs: showing the tip of optical fiber patterned with an Al hole array (a) fiber in ferrule (b) close-up and (c) magnified image of the individual holes.

sensors (this work being a first step to the parallel fabrication of multiple sensors). In addition, while aluminum has slightly greater losses in the SWIR the losses are manageable. Aluminum forms a native oxide that limits tarnishing similar to gold. However, aluminum does not have interband transitions limiting its performance at shorter wavelengths. Figure 2 shows the SEM micrographs for different hole sizes.

One advantage of MPL is that the diameter of the holes in the photoresist can be controlled by adjusting the UV exposure dose. Figure 3 shows this dependence for a 50 nm thick Al film deposited and patterned on the fiber tip. The photoresist was thinned with PGMEA and spun to a thickness of 120 nm. MPL was performed using p = 1 μm spheres and the photoresist was developed for 7 s (120 nm photoresist thickness). The diameter of the holes is very sensitive to small changes in the dose at the low exposure doses required to create smaller holes. This sensitivity is lower for larger holes.

III. COMPUTATIONAL ANALYSIS

The frequency-domain finite-element method (Ansys Electronics Desktop) is used to model a hexagonal close-packed (HCP) hole array defined in an aluminum film. Infinitely periodic boundary conditions are used to model the array. This neglects any truncation effects at defects or at the edge of the core. The hole array is excited with a normally incident

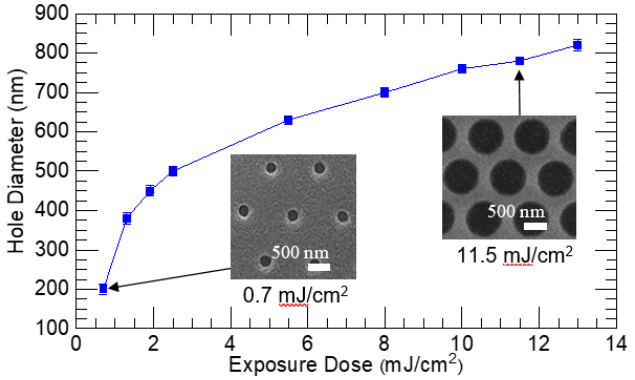

FIGURE 3. Schematic of hole pattern on fiber tip: the upper part shows the microsphere assembled on the fiber tip before exposure, (photoresist layer was ignored in the schematic); the lower part shows the al hole pattern after etching.

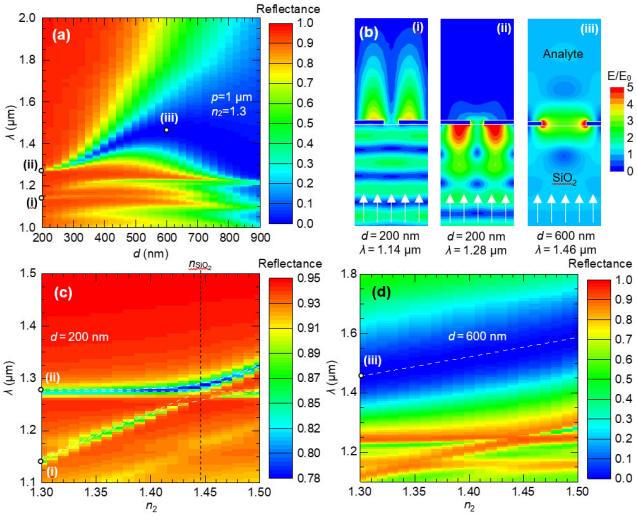

FIGURE 4. (a) Reflection spectra with respect to hole diameters on 50 nm thick Al layer for n2 = 1.3; (b) E-field distributions for three points in (a,c-d), Reflection spectra for (c) d = 200 nm and (d) d = 600 nm holes with varied analyte index, n2.

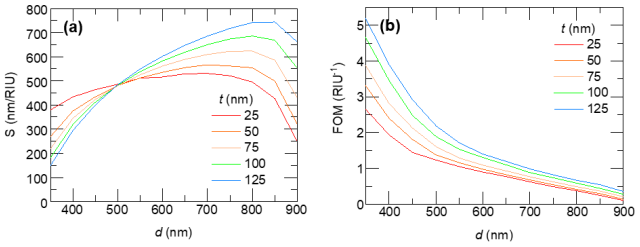

FIGURE 5. (a) Sensitivity S with respect to different d and t within the RI range from 1.3 to 1.4. (b) FOM with respect to different diameters d and t within the RI range from 1.3 to 1.4.

plane wave from the silica side of the film which represents the low numerical aperture illumination propagating in the single-mode optical fiber. The side that has the sensing film is then immersed in the analyte and simulated with a range of optical indices, n_2. Figure 4a shows the simulated reflection spectra for different hole diameter (d), on 50 nm thick (t) Al film in a HCP pitch ($p = 1\ \mu$m). Different modes are evident for $n_2 = 1.3$ (water). Figure 4b shows the field distribution the three instances labeled (i)-(iii) in Figure. 4a. Figure 4c shows diffractive/LRSP modes are bound to the Al/analyte interface at $\lambda = 1.14\ \mu$m (i) and to the SiO_2/Al interface at $\lambda = 1.22\ \mu$m (ii), for the $d = 200$ nm holes. As n_2 increases, the LSPR mode bound to the Al/analyte interface (i) occurs at longer wavelengths, while the one at the SiO_2/Al interface (ii) does not change significantly which agrees with Fig. 4b, showing minimal field penetration into the analyte for this condition (ii). A Rabi-splitting type anti-crossing can be observed as n_2 of analyte approaches the refractive index of SiO_2 at $n_2 = 1.44$. The sensitivity of the bound Al/analyte mode is high; 954 nm/RIU at $n_2 = 1.33$, however, the coupling is low, and the resonant wavelength is determined by the periodicity (the diameter of the microspheres) as opposed to the geometry.

Figure 4a shows that the SiO_2/Al interface bound mode (ii) couples to a waveguide mode in the holes (iii) with the resonant wavelength scaling with the hole diameter. Figure 4d shows how the reflection spectra evolves with changing the analyte index of refraction. The sensitivity of this mode is 601 nm/RIU. The resonance occurs near the cutoff wavelength for the TE_{11} mode in the circular waveguide ($\lambda_c = 1.71 \cdot d \cdot n$) but the sensitivity is lower than would be expected ($d\lambda_c/dn = 1020$ nm/RIU) as a result of the influence of coupling and the fact that much the field distribution at resonance lies in the SiO_2.

The thickness of the aluminum film, t, also influences the sensitivity. In general, thicker films correspond to a greater sensitivity. This is illustrated in Figure 5. The FOM also increases with film thickness as the response becomes more dependent on coupling to the analyte filled waveguide at cutoff. However, since Al wet etching is isotropic. Etching a thicker layer would result in tapered hole which would remove some of the benefits shown in simulation. In the future, we will develop procedures for thicker Al layers and modify the simulation results to accommodate tapered sidewalls.

IV. REFRACTIVE INDEX MEASUREMENT

The experimental setup that was used to test the device is illustrated in Figure 6. A four LED wide band light source (Agilent 83437A) with a spectral range (1250 nm - 1650 nm limited by the equipment) is coupled through a single-mode optic coupler to the patterned fiber tip. Reflected light from the fiber tip is reflected back through the bifurcated cable and is collected by an Optical Spectrum Analyzer (AQ6317B) (OSA). The spectral shift measured by the OSA corresponds to the change of the refractive index of the light through the medium where the sensor is placed. The pattern on fiber tip is the small holes in a thin deposited aluminum layer as previously described.

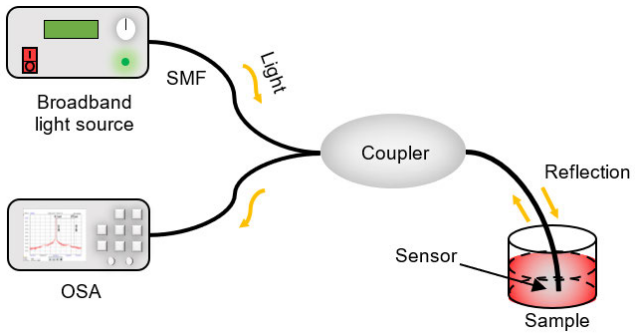

FIGURE 6. Testing Setup of the Biochemical Sensor: the setup has a light source, bifurcated single-mode fiber cable, our sensor, and a light spectrum analyzer.

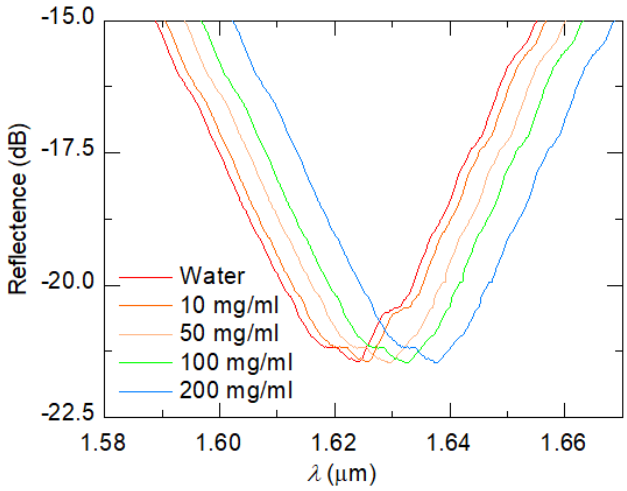

FIGURE 7. Testing Result: Reflection spectra that recorded in water and different concentrations of glucose in water.

Losses can occur during the measurement because of slight differences in the hole diameters or spacing though SEM images show that these differences are minimal. Other losses may come from coupling the fiber sensor to the interrogation setup (broadband source and OSA). The biggest apparent losses (larger quality factor) are that the sensors targeted a waveguide based resonant mode in the sensor as opposed to the plasmonic/diffractive mode commonly exploited in sensors.

Fig. 7 shows the measured reflection spectra measured from a sensor with d = 600 nm holes defined in a t = 50 nm film when the fiber tip is immersed in different glucose/water concentrations. The measured resonance occurs at $\lambda_0 = 1.62\ \mu$m for distilled water and is red shifted as the glucose concentration increases.

The refractive index was calculated according to the linear relationship between glucose concentration and refractive index [43]. Figure 8 shows the shift in resonant wavelength with respect to the calculated refractive index of glucose solution. The resonant wavelength shifted $\Delta\lambda = 48$ nm as refractive index changed from 1.3328 to 1.4101. Higher

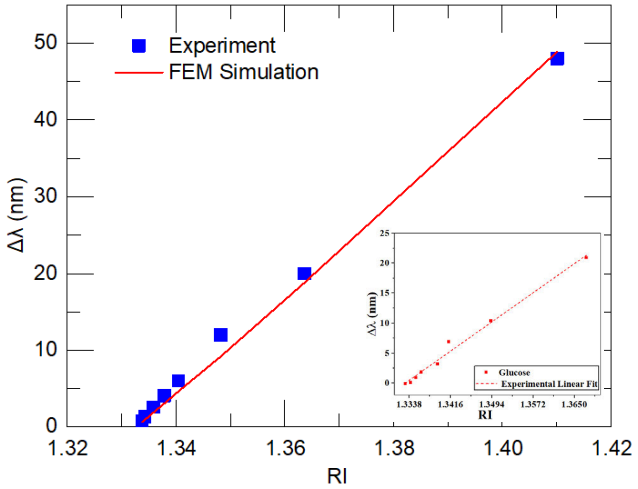

FIGURE 8. Comparison of Sensitivity from Experiment and Simulation: hole size d = 600 nm and metal thickness t = 50 nm. Inserted show the linear fit of the testing result from 0 to 200 mg/ml glucose concentration. The slope of the linear fit is 613 nm/RIU which represent the testing sensitivity of the sensor.

glucose concentrations were tested but they are not presented because high concentrations would cause the low concentrations to be suppressed in the figure. A sensitivity of 613 nm/RIU is measured from a linear fit of the experimental data (Figure 8 insert). This agrees with simulated results S = 632 nm/RIU. While the sensitivity is competitive, the simulations predict that greater sensitivity could be achieved using the bound propagating mode within the measurement range. The good agreement between the simulated results for an infinite array of holes, illustrate the robustness of the waveguide mode-based sensor including the insensitivity to any truncation effects resulting from the finite number of holes are illuminated by the core of the fiber as well as any defects in the self-assembly.

Stability has been verified by repeating measuring the same fiber for many times. The result shows the sensor is very stable and consistent during testing in various experiments. Future work will study the repeatability of the fabrication process. Previous studies of MPL have shown good consistency over much greater areas. While there are slight variations in any university laboratory process, initial fabrication runs have shown reasonable repeatability.

V. CONCLUSION

This work demonstrated the use of Microsphere Photolithography to create a simple refractive index sensor. A waveguide mode resonator pattern on the end-facet of an optical fiber is sensitive to changes in the glucose concentration. The principal appeal of this approach is that it can be scaled to simultaneously pattern multiple fibers in parallel with minimal variability. The approach can be readily tuned to produce different spectra by adjusting the resonator patterns. This is achievable by adjusting the exposure dose and angle of incidence of the illumination. The periodicity of the resonator

is dependent on the microsphere diameter and thus can also be easily adjusted. Future work will be improving the sensitivity and FOM of the resonators by exploiting bound diffractive modes as well as creating resonators with high local field concentrations at specific wavelengths for non-linear spectroscopy techniques such as Surface Enhanced Raman Spectroscopy (SERS).

ACKNOWLEDGMENT

The authors declare no conflicts of interest.

Ibrahem Jasim and Jiayu Liu have equal contributions in the experiment and writing–original draft. Chen Zhu is responsible for the simulations and modeling. Ibrahem Jasim, Jiayu Liu, and Chen Zhu have the equal contributions to this project and article. Muhammad Roman and Jie Huang provided the equipment and laboratory for conducting the experiments.

REFERENCES

[1] S. Enoch and N. Bonod, *Plasmonics: From Basic to Advanced Topics* (Springer Series in Optical Sciences), vol. 167. Jul. 2012, p. 321.
[2] E. J. Smythe, M. D. Dickey, B. Jiming, G. M. Whitesides, and F. Capasso, "Optical antenna arrays on a fiber facet for *in situ* surface-enhanced Raman scattering detection," *Nano Lett.*, vol. 9, no. 3, pp. 1132–1138, 2009.
[3] Y. Liang, Z. Yu, L. Li, and T. Xu, "A self-assembled plasmonic optical fiber nanoprobe for label-free biosensing," *Sci. Rep.*, vol. 9, p. 1, May 2019.
[4] J. Jatschka, A. Dathe, A. Csáki, W. Fritzsche, and O. Stranik, "Propagating and localized surface plasmon resonance sensing—A critical comparison based on measurements and theory," *Sens. Bio-Sens. Res.*, vol. 7, pp. 62–70, Mar. 2016.
[5] A. Iadicicco, S. Campopiano, A. Cutolo, M. Giordano, and A. Cusano, "Refractive index sensor based on microstructured fiber Bragg grating," *IEEE Photon. Technol. Lett.*, vol. 17, no. 6, pp. 1250–1252, Jun. 2005.
[6] J. Wo, G. Wang, Y. Cui, Q. Sun, R. Liang, P. P. Shum, and D. Liu, "Refractive index sensor using microfiber-based Mach–Zehnder interferometer," *Opt. Lett.*, vol. 37, no. 1, pp. 67–69, 2012.
[7] D. K. C. Wu, B. T. Kuhlmey, and B. J. Eggleton, "Ultrasensitive photonic crystal fiber refractive index sensor," in *Proc. Opt. InfoBase Conf. Paper*. Washington, DC, USA: Optical Society America, 2009, pp. 322–324.
[8] V. D. Ta, R. Chen, L. Ma, Y. J. Ying, and H. D. Sun, "Whispering gallery mode microlasers and refractive index sensing based on single polymer fiber," *Laser Photon. Rev.*, vol. 7, no. 1, pp. 133–139, 2013.
[9] Y. Xu, P. Bai, X. Zhou, Y. Akimov, C. E. Png, L. Ang, W. Knoll, and L. Wu, "Optical refractive index sensors with plasmonic and photonic structures: Promising and inconvenient truth," *Adv. Opt. Mater.*, vol. 7, no. 9, 2019, Art. no. 1801433.
[10] A. J. Haes and R. P. Van Duyne, "A unified view of propagating and localized surface plasmon resonance biosensors," *Anal. Bioanal. Chem.*, vol. 379, pp. 920–930, Jul. 2004.
[11] J. Homola, S. S. Yee, and G. Gauglitz, "Surface plasmon resonance sensors," *Sens. Actuators, B Chem.*, vol. 54, pp. 3–15, Jan. 1999.
[12] S. J. Zalyubovskiy, M. Bogdanova, A. Deinega, Y. Lozovik, A. D. Pris, K. H. An, W. P. Hall, and R. A. Potyrailo, "Theoretical limit of localized surface plasmon resonance sensitivity to local refractive index change and its comparison to conventional surface plasmon resonance sensor," *J. Opt. Soc. Amer. A, Opt. Image Sci.*, vol. 29, no. 6, pp. 994–1002, 2012.
[13] C. Yu and J. Irudayaraj, "Quantitative evaluation of sensitivity and selectivity of multiplex nanoSPR biosensor assays," *Biophys. J.*, vol. 93, pp. 3684–3692, Nov. 2007.
[14] D. P. Lyvers, J. M. Moon, A. V. Kildishev, V. M. Shalaev, and A. Wei, "Gold nanorod arrays as plasmonic cavity resonators," *ACS Nano*, vol. 2, no. 12, pp. 2569–2576, 2008.
[15] H. Chen, X. Kou, Z. Yang, W. Ni, and J. Wang, "Shape- and size-dependent refractive index sensitivity of gold nanoparticles," *Langmuir*, vol. 24, no. 10, pp. 5233–5237, 2008.
[16] H. Wang, D. W. Brandl, F. Le, P. Nordlander, and N. J. Halas, "Nanorice: A hybrid plasmonic nanostructure," *Nano Lett.*, vol. 6, no. 4, pp. 827–832, 2006.
[17] Y. Shen, J. Zhou, T. Liu, Y. Tao, R. Jiang, M. Liu, G. Xiao, J. Zhu, Z. K. Zhou, X. Wang, C. Jin, and J. Wang, "Plasmonic gold mushroom arrays with refractive index sensing figures of merit approaching the theoretical limit," *Nat. Commun.*, vol. 4, no. 1, pp. 1–9, 2013.
[18] P. Bhatia and B. D. Gupta, "Surface-plasmon-resonance-based fiber-optic refractive index sensor: Sensitivity enhancement," *Appl. Opt.*, vol. 50, no. 14, pp. 2032–2036, 2011.
[19] P. Jia and J. Yang, "Integration of large-area metallic nanohole arrays with multimode optical fibers for surface plasmon resonance sensing," *Appl. Phys. Lett.*, vol. 102, no. 24, 2013, Art. no. 243107.
[20] X. He, H. Yi, J. Long, X. Zhou, J. Yang, and T. Yang, "Plasmonic crystal cavity on single-mode optical fiber end facet for label-free biosensing," *Appl. Phys. Lett.*, vol. 108, no. 23, 2016, Art. no. 231105.
[21] X. Lan, B. Cheng, Q. Yang, J. Huang, H. Wang, Y. Ma, H. Shi, and H. Xiao, "Reflection based extraordinary optical transmission fiber optic probe for refractive index sensing," *Sens. Actuators B, Chem.*, vol. 193, pp. 95–99, Mar. 2014.
[22] A. Dhawan, J. F. Muth, D. N. Leonard, M. D. Gerhold, J. Gleeson, T. Vo-Dinh, and P. E. Russell, "Focused ion beam fabrication of metallic nanostructures on end faces of optical fibers for chemical sensing applications," *J. Vac. Sci. Technol. B Microelectron. Nanometer Struct. Process., Meas., Phenomena*, vol. 26, no. 6, pp. 2168–2173, 2008.
[23] Y. Lin, Y. Zou, Y. Mo, J. Guo, and R. G. Lindquist, "E-beam patterned gold nanodot arrays on optical fiber tips for localized surface plasmon resonance biochemical sensing," *Sensors*, vol. 10, no. 10, pp. 9397–9406, 2010.
[24] Y. Lin, Y. Zou, and R. G. Lindquist, "A reflection-based localized surface plasmon resonance fiber-optic probe for biochemical sensing," *Biomed. Opt. Exp.*, vol. 2, no. 3, pp. 478–484, 2011.
[25] M. Consales, A. Ricciardi, A. Crescitelli, E. Esposito, A. Cutolo, and A. Cusano, "Lab-on-fiber technology: Toward multifunctional optical nanoprobes," *ACS Nano*, vol. 6, no. 4, pp. 3163–3170, 2012.
[26] S. Feng, S. Darmawi, T. Henning, P. J. Klar, and X. Zhang, "A miniaturized sensor consisting of concentric metallic nanorings on the end facet of an optical fiber," *Small*, vol. 8, no. 12, pp. 1937–1944, 2012.
[27] H. Nguyen, F. Sidiroglou, S. F. Collins, T. J. Davis, A. Roberts, and G. W. Baxter, "A localized surface plasmon resonance-based optical fiber sensor with sub-wavelength apertures," *Appl. Phys. Lett.*, vol. 103, no. 19, 2013, Art. no. 193116.
[28] J. Cao, E. K. Galbraith, T. Sun, and K. T. V. Grattan, "Cross-comparison of surface plasmon resonance-based optical fiber sensors with different coating structures," *IEEE Sensors J.*, vol. 12, no. 7, pp. 2355–2361, Jul. 2012.
[29] S. Shi, L. Wang, R. Su, B. Liu, R. Huang, W. Qi, and Z. He, "A polydopamine-modified optical fiber SPR biosensor using electroless-plated gold films for immunoassays," *Biosensors Bioelectron.*, vol. 74, pp. 454–460, Dec. 2015.
[30] G. Kostovski, U. Chinnasamy, S. Jayawardhana, P. R. Stoddart, and A. Mitchell, "Sub-15 nm optical fiber nanoimprint lithography: A parallel, self-aligned and portable approach," *Adv. Mater.*, vol. 23, no. 4, pp. 531–535, 2011.
[31] M. Pisco, F. Galeotti, G. Quero, G. Grisci, A. Micco, L. V. Mercaldo, P. D. Veneri, A. Cutolo, and A. Cusano, "Nanosphere lithography for optical fiber tip nanoprobes," *Light Sci. Appl.*, vol. 6, no. 5, 2017, Art. no. e16229.
[32] G. Kostovski, P. R. Stoddart, and A. Mitchell, "The optical fiber tip: An inherently light-coupled microscopic platform for micro- and nanotechnologies," *Adv. Mater.*, vol. 26, no. 23, pp. 3798–3820, 2014.
[33] C. Qu and E. C. Kinzel, "Polycrystalline metasurface perfect absorbers fabricated using microsphere photolithography," *Opt. Lett.*, vol. 41, no. 15, pp. 3399–3402, 2016.
[34] W. Wu, D. Dey, O. G. Memis, A. Katsnelson, and H. Mohseni, "Fabrication of large area periodic nanostructures using nanosphere photolithography," *Nanoscale Res. Lett.*, vol. 3, no. 10, pp. 351–354, 2008.
[35] A. Bonakdar, M. Rezaei, R. L. Brown, V. Fathipour, E. Dexheimer, S. J. Jang, and H. Mohseni, "Deep-UV microsphere projection lithography," *Opt. Lett.*, vol. 40, no. 11, pp. 2537–2540, 2015.
[36] Y. C. Chang, S. M. Wang, H. C. Chung, C. B. Tseng, and S. H. Chang, "Observation of absorption-dominated bonding dark plasmon mode from metal–insulator–metal nanodisk arrays fabricated by nanospherical-lens lithography," *ACS Nano*, vol. 6, no. 4, pp. 3390–3396, 2012 .
[37] E. C. Kinzel, C. Qu, and C. Zhu, "Fabrication of infrared broadband polarized emitting metasurfaces using microsphere photolithography," *Proc. SPIE*, vol. 10544, Feb. 2018, Art. no. 105440C.

[38] O. Shavdina, L. Berthod, T. Kämpfe, S. Reynaud, C. Veillas, I. Verrier, M. Langlet, F. Vocanson, P. Fugier, Y. Jourlin, and O. Dellea, "Large area fabrication of periodic TiO_2 nanopillars using microsphere photolithography on a photopatternable sol–gel film," *Langmuir*, vol. 31, no. 28, pp. 7877–7884, 2015.
[39] A. Bonakdar, S. J. Jang, and H. Mohseni, "Novel high-throughput and maskless photolithography to fabricate plasmonic molecules," *J. Vac. Sci. Technol. B, Nanotechnol. Microelectron. Mater. Process. Meas. Phenomena*, vol. 32, no. 2, 2014, Art. no. 20604.
[40] I. Jasim, J. Liu, Y. Yang, C. Qu, C. Zhu, M. Roman, J. Huang, E. C. Kinzel, and M. Almasri, "Low-cost fabrication of functional plasmonic fiber-optic-based sensors using microsphere photolithography," *Proc. SPIE*, vol. 11000, Jun. 2019, Art. no. 110000D.
[41] J. Liu, I. Jasim, M. Roman, Y. Yang, C. Qu, J. Huang, E. Kinzel, and M. Almasri, "Functional plasmonic fiber-optic based sensors using low-cost microsphere photolithography," in *Proc. 20th Int. Conf. Solid-State Sensors, Actuators Microsyst. Eurosensors XXXIII, TRANSDUCERS 2019 EUROSENSORS XXXIII*. Piscataway, NJ, USA: Institute Electrical Electronics Engineers, Jun. 2019, pp. 1545–1548.
[42] X. Meng and D. Qiu, "Gas-flow-induced reorientation to centimeter-sized two-dimensional colloidal single crystal of polystyrene particle," *Langmuir*, vol. 30, no. 11, pp. 3019–3023, 2014.
[43] C. Y. Tan and Y. X. Huang, "Dependence of refractive index on concentration and temperature in electrolyte solution, polar solution, nonpolar solution, and protein solution," *J. Chem. Eng. Data*, vol. 60, no. 10, pp. 2827–2833, 2015.

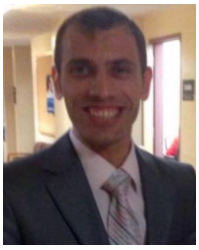

IBRAHEM JASIM is currently pursuing the Ph.D. degree with five years practical experience in semiconductor processing, photolithography, cleanroom environment operation, MEMS fabrication, microfluidics, plasma etching, thin film, spectroscopy, equipment (operation, maintenance, training, troubleshooting, and fixing), laboratory management, and strong educational background. He has C++ CUDA programming and Verilog hardware design experience. He seeks to bring further success to firm through dedication, exceptional focus, and hard work.

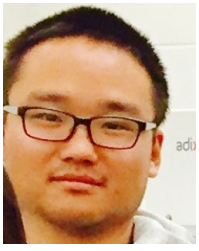

JIAYU LIU is currently pursuing the Ph.D. degree in electrical and computer engineering with the University of Missouri, Columbia. His research interests include biosensors and microfluidics for foodborne pathogen detection, fiber-optic sensor, and microsphere photo lithography on fiber tip.

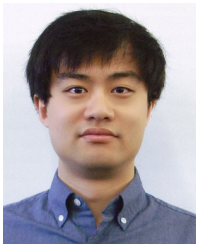

CHEN ZHU received the B.S. degree from Wuhan University, in 2013, and the master's degree from USTC, China, in 2017. He is currently pursuing the Ph.D. degree with the Department of Aerospace and Mechanical Engineering, University of Notre Dame, IN, USA. His research interests include nanoscale fabrication and optics particularly toward controlling heat transfer.

MUHAMMAD ROMAN is currently pursuing the Ph.D. degree in electrical engineering with the Missouri University of Science and Technology, Rolla, MO, USA. His research interests include design and development of distributed fiber-optic sensors for temperature and strain measurements in harsh environments.

JIE HUANG (Senior Member, IEEE) research interests include fiber optic sensors; novel photonic/microwave micro/nano materials, structures, devices, and sensors; ultrafast laser machining, processing, and characterization of micro/nano structures, materials, and devices; sensors and instrumentation for applications in harsh environments; microwave-photonic sensing, imaging, and spectroscopy; and optical biomedical imaging and sensing (photoacoustic tomography/spectroscopy).

EDWARD KINZEL research interests include laser/material interaction with a focus on manufacturing/fabrication as well as sensing and energy harvesting.

MAHMOUD ALMASRI is currently an Associate Professor with the Department of Electrical Engineering and Computer Science, University of Missouri. His research and published materials include uncooled infrared microblometers, micromirrors, Coulter counter, micropost array for mapping cell traction forces, wafer level packaging, and 3-D microscaffolds for brain slice and neuronal networks studies *in vitro* and *in situ*.